Magnetic properties and spin dynamics in the spin-orbit driven $J_{\text{eff}} = \frac{1}{2}$ triangular lattice antiferromagnet $Ba_6Yb_2Ti_4O_{17}$

J. Khatua,[1] S. Bhattacharya,[2] A. M. Strydom,[3] A. Zorko,[4,5] J. S. Lord,[6] A. Ozarowski,[7] E. Kermarrec,[2] and P. Khuntia[1,8,*]

[1]*Department of Physics, Indian Institute of Technology Madras, Chennai 600036, India*
[2]*Laboratoire de Physique des Solides, Université Paris-Saclay, CNRS, F-91405 Orsay, France*
[3]*Highly Correlated Matter Research Group, Department of Physics, University of Johannesburg, P.O. Box 524, Auckland Park 2006, South Africa*
[4]*Jožef Stefan Institute, Jamova cesta 39, SI-1000 Ljubljana, Slovenia*
[5]*Faculty of Mathematics and Physics, University of Ljubljana, Jadranska ulica 19, SI-1000 Ljubljana, Slovenia*
[6]*ISIS Facility, STFC Rutherford Appleton Laboratory, Didcot OX11 0QX, United Kingdom*
[7]*National High Magnetic Field Laboratory, Florida State University, Tallahassee, Florida 32310, USA*
[8]*Quantum Centre of Excellence for Diamond and Emergent Materials, Indian Institute of Technology Madras, Chennai 600036, India*

(Received 3 November 2023; accepted 4 January 2024; published 19 January 2024)

Frustration-induced strong quantum fluctuations accompanied by spin-orbit coupling and crystal electric field can give rise to rich and diverse magnetic phenomena associated with unconventional low-energy excitations in rare-earth-based quantum magnets. Herein, we present crystal structure, magnetic susceptibility, specific heat, muon spin relaxation (μSR), and electron spin resonance (ESR) studies on polycrystalline samples of $Ba_6Yb_2Ti_4O_{17}$, in which Yb^{3+} ions constitute a perfect triangular lattice in the *ab* plane without detectable antisite disorder between atomic sites. The Curie-Weiss fit of the low-temperature magnetic susceptibility data suggests spin-orbit driven effective pseudospin $J_{\text{eff}} = \frac{1}{2}$ degrees of freedom of Yb^{3+} spin with weak antiferromagnetic exchange interactions in the Kramers doublet ground state. The zero-field specific heat data reveal the presence of long-range magnetic order at Néel temperature $T_N = 77$ mK which is suppressed in a magnetic field $\mu_0 H \geqslant 1$ T. The broad maximum in specific heat is attributed to the Schottky anomaly implying the Zeeman splitting of the Kramers doublet ground state in a magnetic field. The ESR measurements suggest the presence of anisotropic exchange interaction between the moments of Yb^{3+} spins. The μSR experiments reveal a fluctuating state of Yb^{3+} spins in the temperature range $0.1\ \text{K} \leqslant T \leqslant 10$ K owing to depopulation of crystal electric field levels, which suggests that the lowest Kramers doublets with $J_{\text{eff}} = \frac{1}{2}$ are well separated, and the low-temperature physics of this frustrated magnet is dominated by $J_{\text{eff}} = \frac{1}{2}$ moments. In addition to the intraplane nearest-neighbor superexchange interaction, the interplane exchange interaction and anisotropy are expected to stabilize the long-range ordered state in this triangular lattice antiferromagnet.

DOI: 10.1103/PhysRevB.109.024427

I. INTRODUCTION

Quantum materials wherein the interplay between competing degrees of freedom, frustration-induced strong quantum fluctuations, and quantum entanglement is prominent have drawn considerable attention due to their connection to the emergence of exotic quantum phenomena with potential to address some of the recurring themes in quantum condensed matter physics [1–6]. One noteworthy example is the quantum spin liquid (QSL), in which strongly entangled electron spins do not exhibit long-range magnetic order down to absolute zero temperature despite strong spin correlations [7,8]. Originally, the QSL state was proposed by Anderson for a system composed of $S = \frac{1}{2}$ spins on a two-dimensional triangular lattice antiferromagnet [9]. Its materialization has been proposed in a few triangular lattice antiferromagnets with next-nearest-neighbor interaction and anisotropic exchange interaction [10–15]. Furthermore, the quantum nature of this entangled state offers an outstanding track to study gauge theories incorporating fractionalized excitations, as well as its relevance in the field of quantum computing [16–18]. Despite the fact that several QSL candidate materials show analogous behavior in various observables [19–23], understanding the microscopic spin Hamiltonian to identify fractionalized excitations remains a significant challenge because of the presence of extra exchange couplings, intrinsic disorder, and unavoidable defects in real materials [12,17,24–26].

In this context, rare-earth-based materials featuring $J_{\text{eff}} = \frac{1}{2}$ quantum spins decorated on geometrically frustrated lattices offer a promising avenue for the experimental realization of exotic quantum phenomena [11,23,27–31]. Moreover, it has been suggested that anisotropic magnetic interactions between $J_{\text{eff}} = \frac{1}{2}$ moments in the Kramers crystal field ground state of these magnetic materials play an important role in the materialization of the QSL state, in contrast to isotropic interactions between pure $S = \frac{1}{2}$ moments in the triangular lattice Heisenberg model, which tend to promote a 120°

*pkhuntia@iitm.ac.in

long-range magnetic ordered state [32]. For example, the rare-earth triangular antiferromagnets $YbMgGaO_4$ [33–35] and chalcogenides $NaYbC_2$ (C = O, S, Se) [36–43] with Yb^{3+} ions with $J_{\text{eff}} = \frac{1}{2}$ moment have attracted considerable interest due to the emergence of a QSL ground state brought about by the presence of dominant easy-plane anisotropic magnetic interactions and spin frustration [44,45]. In contrast to the QSL state with dominant easy-plane anisotropic magnetic interactions, spin-liquid candidates on a structurally perfect triangular lattice with dominant easy-axis anisotropy are very rare [46] and have been found only very recently in $NdTa_7O_{19}$, which appears to be the first realization of a spin-liquid ground state with Ising-like magnetic correlations driven by strong easy-axis anisotropic magnetic interaction [11,47]. Furthermore, the impact of dipolar magnetic interactions on the observed spin excitation continuum, widely considered as the most robust evidence of spin fractionalization in insulators, remains a dynamic and actively researched domain in quantum condensed matter physics [48,49].

In addition to the anisotropic exchange interactions, there have been proposals for a dominant dipolar-interaction-driven spin-liquid state in certain triangular lattice antiferromagnets, such as $Yb(BaBO_3)_3$ [50–52] and $ABaYb(BO_3)_2$ (A = Na, K) [53,54]. In addition to their dynamic ground states, the phase transitions observed in triangular lattice antiferromagnets are of significant interest for gaining insights into intriguing quantum phenomena such as Berezinskii-Kosterlitz-Thouless (BKT) physics [55,56]. For example, the observed quasi-long-range magnetic ordered state in the two-dimensional triangular lattice material $TmMgGaO_4$ may represent the manifestation of the BKT phase [57–59]. Recently, it has been suggested that the dipolar spin-liquid candidate $KBaGd(BO_3)_2$ is a promising candidate to host a BKT phase and an unconventional quantum critical point [60]. Furthermore, rare-earth-based magnets with weakly coupled magnetic moments, approaching the paramagnetic limit, have shown potential for lowering system temperatures through adiabatic demagnetization cooling, as observed in triangular lattice antiferromagnets such as $KBaGd(BO_3)_2$ [61] and $KBaYb(BO_3)_2$ [62]. Interestingly, in such rare-earth quantum magnets, anisotropic magnetic interaction induced by spin-orbit coupling, the crystal electric field of localized $4f$ electrons, and lattice symmetry offers a viable platform to host unconventional phases including a spiral spin liquid [63,64]. In a similar vein, a Kitaev spin-liquid state induced by bond-dependent anisotropic magnetic interactions [65–67] and multipolar orders [68] in spin-orbit driven $J_{\text{eff}} = \frac{1}{2}$ quantum magnets remains largely unexplored. The current effort is devoted towards the design, discovery, and investigation of two- and three-dimensional spin-orbit driven $4f$-based frustrated magnets' potential to host myriads of exotic quantum phases that may aid in the establishment of new theoretical paradigms in quantum condensed matter physics. In order to realize a rich variety of spin-orbit driven quantum phenomena as a result of competing exchange interaction, crystal electric field, and anisotropic interaction, it is therefore essential to explore disorder-free rare-earth-based quantum magnets.

Herein, we report the crystal structure and magnetic properties of an unexplored triangular lattice antiferromagnet $Ba_6Yb_2Ti_4O_{17}$ (henceforth, BYTO), which crystallizes in the hexagonal space group $P6_3/mmc$ where the Yb^{3+} ions constitute a perfect triangular lattice in the ab plane. The Rietveld analysis of x-ray diffraction (XRD) data reveals the absence of antisite disorder between the crystallographic sites. Magnetic susceptibility data suggest that Yb^{3+} spins acquire $J_{\text{eff}} = \frac{1}{2}$ degrees of freedom and the presence of a weak antiferromagnetic exchange interaction between rare-earth moments. The zero-field specific heat data show an anomaly possibly due to the long-range magnetic order at Néel temperature $T_N = 77$ mK which disappears in a magnetic field $\mu_0 H \geqslant 1$ T. Muon spin relaxation (μSR) experiments suggest the lack of long-range magnetic order down to 80 mK, while spin fluctuations are observed up to 10 K. The anisotropic magnetic exchange interaction between $J_{\text{eff}} = \frac{1}{2}$ moments of Yb^{3+} spins was suggested from electron spin resonance measurements. The combination of magnetic anisotropy and intraplane and interplane exchange interactions is expected to stabilize a long-range magnetic ordered state in this antiferromagnet.

II. EXPERIMENTAL DETAILS

Polycrystalline samples of BYTO were prepared by a conventional solid-state method. Prior to use, we preheated stoichiometric amounts of $BaCO_3$ (Alfa Aesar, 99.997%), and Yb_2O_3 (Alfa Aesar, 99.998%) at 200 and 800 °C, respectively, to prevent moisture contamination. Afterward, we combined them with a stoichiometric amount of TiO_2 (Alfa Aesar, 99.995%) to get a homogeneous mixture. The stoichiometric mixtures were pelletized and sintered at 1400 °C for 72 h with several intermittent grindings. The phase purity of the final product was confirmed by x-ray diffraction at 300 K employing a Rigaku smartLAB x-ray diffractometer with Cu Kα radiation ($\lambda = 1.54$ Å). Magnetization measurements were carried out using a Quantum Design (San Diego, CA) superconducting quantum interference device [SQUID; Magnetic Property Measuring System (MPMS)] in the temperature range 2 K $\leqslant T \leqslant$ 350 K in several magnetic fields. Specific heat measurements were performed using a Quantum Design Physical Property Measurement System (PPMS) in the temperature range 2 K $\leqslant T \leqslant$ 270 K and in magnetic fields up to 7 T. In addition, specific heat measurements were carried out in the temperature range 0.049 K $\leqslant T \leqslant$ 4 K at 0, 1, and 3 T in a dilution refrigerator using a DynaCool PPMS instrument from Quantum Design. Thermal conductivity measurements were conducted in the temperature range 2 K $\leqslant T \leqslant$ 300 K in magnetic fields up to 7 T using the two-probe method also using the Quantum Design PPMS. The μSR experiments in zero field and in longitudinal magnetic fields were performed on the MuSR spectrometer at the ISIS pulsed neutron and muon source at Rutherford Appleton Laboratory (Didcot, UK). The powder sample (∼1 g) was mixed with a small amount of GE-varnish and fixed to a silver plate. A 25-μm-thick silver foil was placed on top of the sample to maximize the number of implanted muons in the sample and to reduce the thermal radiation. A dilution fridge was used for the temperature range 0.08–4 K, and subsequently a helium flow cryostat was used to reach temperatures from 1.4 to 300 K. Electron spin resonance (ESR) measurements were performed at the National High Magnetic Field Laboratory

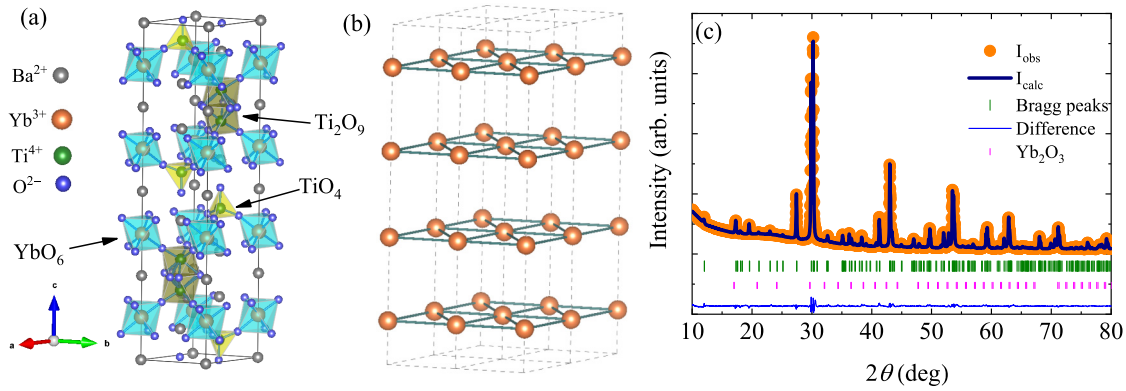

FIG. 1. (a) Schematics of the unit cell of $Ba_6Yb_2Ti_4O_{17}$. The oxygen atoms coordinate with Yb^{3+} ions in an octahedral arrangement (blue). Two top and bottom layers of YbO_6 octahedra are connected through Ti_2O_9 double octahedra, while two middle layers of YbO_6 are connected through TiO_4 tetrahedra. (b) Two-dimensional triangular layers of Yb^{3+} ions arranged in the unit cells. (c) The Rietveld refinement of powder x-ray diffraction data recorded at room temperature. The experimentally observed points (scattered orange points), the calculated Rietveld refinement profile (thick, solid navy curve), the Bragg reflection positions of BYTO (olive vertical bars), the Bragg reflection position of Yb_2O_3 (pink bars), and the difference between observed and calculated intensities (thin, solid blue curve) are shown.

(Tallahassee, FL) on a polycrystalline sample using a custom-made transmission-type ESR spectrometer with homodyne detection. The measurements were conducted in the Faraday configuration at an irradiation frequency of 212 GHz. The magnetic field was swept between 2 and 10 T using a superconducting magnet, and the temperature was varied between 5 and 200 K using a continuous-flow He cryostat. A standard field-modulation technique was used with a modulation field of about 2 mT.

III. RESULTS

A. Rietveld refinement and crystal structure

To examine the phase purity and crystal structure, we carried out the Rietveld refinement of room temperature x-ray diffraction data using General Structure Analysis System (GSAS) software [69]. The XRD results suggest that the polycrystalline BYTO samples contain a tiny fraction of unreacted magnetic Yb_2O_3 impurity, which has a minimal influence on the overall magnetic properties of the material under examination. A similar situation with the unavoidable Yb_2O_3 secondary phase in polycrystalline samples has been observed in a few other Yb-based magnets [70–72]. To accurately determine the percentages of the main and secondary phases, a two-phase Rietveld refinement was performed. The crystallographic parameters of the isostructural compound $Ba_6Y_2Ti_4O_{17}$ were incorporated as a reference to perform the Rietveld refinement for the main phase [73]. Figure 1(c) depicts the Rietveld refinement pattern of the x-ray diffraction data indicating that our polycrystalline samples consist of 98.5% BYTO and 1.5% Yb_2O_3 phases. The Rietveld refinement results indicate that the compound BYTO crystallizes in the 12*H* hexagonal structure with space group $P6_3/mmc$ without intersite mixing between constituent ions. The obtained lattice parameters are $a = b = 5.907$ Å, $c = 29.426$ Å, $\alpha = \beta = 90°$, and $\gamma = 120°$. The estimated fractional atomic coordinates and *R* factors are summarized in Table I.

Figure 1(a) depicts the refined crystal structure of BYTO drawn using Visualization for Electronic and Structural Analysis (VESTA) software [74]. The nearest-neighbor magnetic Yb^{3+} ion (Yb-Yb $\approx$ 5.907 Å) constitutes two-dimensional triangular layers stacked along the *c* axis [see Fig. 1(b)], which is similar to the extensively studied triangular lattice antiferromagnet $YbMgGaO_4$ with an Yb-Yb distance of approximately 3.4 Å [33]. As shown in Fig. 1(b), one unit cell of BYTO is composed of four triangular layers of Yb^{3+} ions where the first two and last two layers from the bottom are separated by an interplanar distance of 7.26 Å while the middle two layers are separated by an interplanar distance of 7.45 Å. In BYTO, the Yb^{3+} ion occupies a single crystallographic site (4*e*) of the hexagonal lattice and forms a distorted YbO_6 tetrahedron [see Fig. 1(a)] with local O^{2-} ions. Due to such an octahedral environment, Yb^{3+} ions are exposed to a strong crystal electric field, which splits the degenerate multiplet of

TABLE I. Refined structural parameters based on x-ray diffraction data at 300 K (space group $P6_3/mmc$, $\alpha = \beta = 90.0°$, $\gamma = 120.0°$, $a = b = 5.907$ Å, $c = 29.426$ Å, $\chi^2 = 4.22$, weighted-profile *R* factor $R_{wp} = 5.88$, unweighted-profile *R* factor $R_p = 3.39$, and expected *R* factor $R_{exp} = 2.86$).

Atom	Wyckoff position	*x*	*y*	*z*	Occupancy
Yb	4*e*	0	0	0.126	1
Ba_1	2*a*	0	0	0	1
Ba_2	24*l*	0.666	0.333	0.089	1
Ba_3	24*l*	0.333	0.666	0.182	1
Ba_4	2*b*	0	0	0.25	1
Ti_1	12*k*	0.666	0.333	−0.055	1
Ti_2	12*k*	0.666	0.333	0.203	1
O_1	12*k*	0.666	0.333	−0.006	1
O_2	12*k*	−0.347	−0.173	0.077	1
O_3	12*k*	0.346	0.173	−0.170	1
O_4	12*j*	0.573	0.014	0.25	1

TABLE II. Some promising rare-earth-based frustrated triangular lattice antiferromagnets and their ground-state magnetic properties.

Material	Symmetry	Exchange path	θ_{CW} at low T (K)	μ_{eff} at low T (μ_B)	T_N (K)	Ref.
$YbMgGaO_4$	$R\bar{3}m$	Yb-O-Yb	−4	2.8		[33,77]
$NaYbO_2$	$R\bar{3}m$	Yb-O-Yb	−5.6	2.84		[41]
$NaBaYb(BO_3)_2$	$R\bar{3}m$	Yb-O-B-O-Yb	−0.069	2.23	0.41	[53]
$K_3Yb(VO_4)_2$	$P6_3m$	Yb-O-V-O-Yb	−1	2.41		[78]
$NdTa_7O_{19}$	$P\bar{6}c2$	Nd-O-Ta-O-Nd	−0.46	1.9		[11]
$Ba_6Yb_2Ti_4O_{17}$	$P6_3/mmc$	Yb-O-Ti-O-Yb	−0.49	2.5	0.077	This paper

$J = \frac{7}{2}$ into four Kramers doublet states of Yb^{3+} ions with spin-orbit driven $J_{eff} = \frac{1}{2}$ moment.

In BYTO, the YbO_6 octahedra are not interconnected through common O^{2-} ions as observed in other triangular lattice antiferromagnets such as $YbMgGaO_4$ or $NaYbX_2$ (X = O, S, Se). Instead, they are linked by TiO_4 tetrahedra, and these form a path for intraplane exchange interactions. On the other hand, the YbO_6 octahedra are connected through Ti_2O_9 dimers for interplane exchange interactions, as illustrated in Fig. 1(a). The larger unit cell of BYTO compared with $YbMgGaO_4$ is the primary reason for the formation of isolated YbO_6 octahedra, which could potentially reduce the strength of intraplane magnetic exchange interactions between the Yb^{3+} moments due to the increased bond length for the f-p-d-p-f (Yb-O-Ti-O-Yb) hybridization.

The presence of weak exchange interactions, resulting from similar superexchange pathways, has been observed in several triangular lattice antiferromagnets, including $NaBaYb(BO_3)_2$ [53], $Ba_3Yb(BO_3)_3$ [52,54], and $Ba_3YbB_9O_{18}$ [29] (as shown in Table II). This scenario differs somewhat for 3d-transition-ion-based magnets, as the electrons of 3d ions are not strongly localized in real space, unlike the 4f ions. For instance, relatively strong exchange interaction between Co^{2+} ions is observed in the 6H-hexagonal spin lattice of $Ba_3CoSb_2O_9$, despite the absence of a common oxygen ligand for intraplane superexchange interactions between the $J_{eff} = \frac{1}{2}$ moments of Co^{2+} ions [75,76]. From a structural perspective, it is worth noting that BYTO and $Ba_3CoSb_2O_9$ share several similarities, aside from differences in their stacking layers [75]. They have similar exchange paths, nearest-neighbor distances of 5.90 Å, and interlayer separations of 7.2 Å. However, the magnetic properties are anticipated to be distinct due to the localized nature and distinct anisotropy of Yb^{3+} ions in BYTO.

B. Magnetic susceptibility

In Fig. 2(a), we show the temperature dependence of magnetic susceptibility $\chi(T)$ in two magnetic fields in the temperature range 2 K $\leqslant T \leqslant$ 350 K. The magnetic susceptibility data do not show any signature of long-range magnetic order at least above 2 K in BYTO. The absence of any marked difference between zero-field-cooled and field-cooled magnetic susceptibility data [see inset of Fig. 2(a)] suggests that Yb^{3+} spins are not frozen at least down to 2 K. In order to calculate the value of the effective magnetic moment μ_{eff} and Curie-Weiss temperature θ_{CW}, the inverse $\chi(T)$ data [see Fig. 2(b)] were fitted by the Curie-Weiss (CW) law $\chi = C/(T - \theta_{CW})$. Here, the Curie constant C is associated with the effective moment through the formula $\mu_{eff} = \sqrt{8C}\ \mu_B$, and θ_{CW} signifies the energy scale of the magnetic exchange interactions between Yb^{3+} moments. The high-temperature CW fit in the temperature range 150 K $\leqslant T \leqslant$ 350 K yields $\theta_{CW} = -102$ K and $\mu_{eff} = 4.57\ \mu_B$. The large negative Curie-

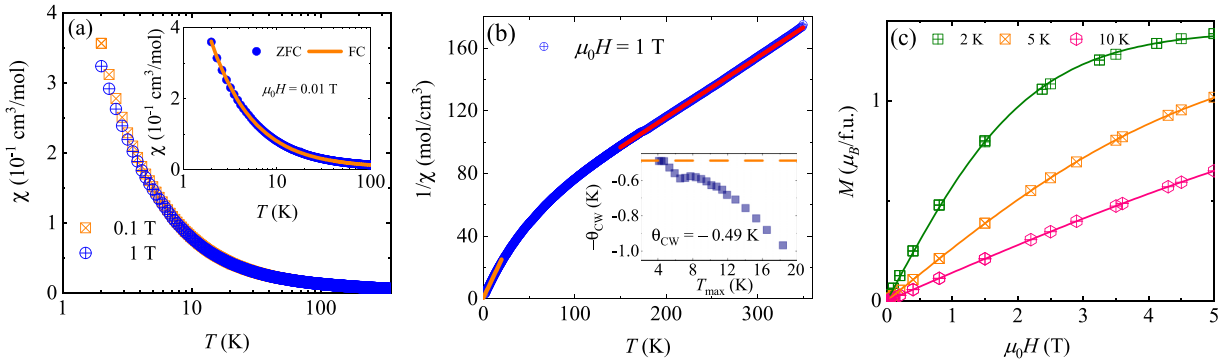

FIG. 2. (a) The temperature dependence of magnetic susceptibility $\chi(T)$ in two different magnetic fields. The inset shows the temperature dependence of zero-field-cooled (ZFC) and field-cooled (FC) magnetic susceptibility measured in μ_0H = 100 Oe. (b) The temperature dependence of inverse magnetic susceptibility [$1/\chi(T)$]. The red and orange lines are the Curie-Weiss fits to the high-temperature and low-temperature inverse magnetic susceptibility data, respectively. The inset shows the estimated Curie-Weiss temperature obtained by varying the upper limit of the temperature range, where the constant value of the Curie-Weiss temperature at low temperature is shown by the dashed orange line. (c) Magnetization as a function of external magnetic field at several temperatures. The solid curves are the Brillouin function fits for paramagnetic Yb^{3+} spins with $J_{eff} = \frac{1}{2}$.

Weiss temperature indicates the presence of elevated energy levels of crystal electric field excitations. The obtained $\mu_{\text{eff}} = 4.57\ \mu_B$ is comparable to the effective moment of free Yb^{3+} ions ($\mu_{\text{eff}}^{\text{free}} = 4.54\ \mu_B$). As previously mentioned, the Yb^{3+} moments are located in an octahedral environment, and as a result, a strong crystal electric field naturally causes the eightfold degenerate $J = \frac{7}{2}$ multiplet to split into four Kramers doublet states.

The preliminary indication of the presence of the ground-state Kramers doublet state can be observed in the temperature-dependent inverse magnetic susceptibility data. In BYTO, we can observe a deviation in the measured susceptibility data from the high-temperature Curie-Weiss fit (indicated by the red line) as depicted in Fig. 2(b), where this deviation becomes noticeable below 100 K. It is important to note that such deviations of measured $\chi(T)$ from the CW fit in transition-metal-based magnets typically reflect the development of magnetic correlations between electronic spins but in rare-earth magnets they are typically due to the presence of crystal electric field excitations.

To gain insights into the Kramers doublet ground state and the nature of magnetic interactions, it is necessary to perform a Curie-Weiss fit at low temperatures sufficiently below the first excited crystal electric field level. It has been brought out in the literature that the Curie-Weiss temperature for rare-earth-based magnets is strongly dependent on the temperature range for the Curie-Weiss fitting, owing to the influence of excited crystal electric field levels [11,72]. To estimate the nature of dominant magnetic interactions between Yb^{3+} moments in the ground-state Kramers doublet of BYTO, we performed fittings of the low-temperature inverse $\chi(T)$ data in various temperature ranges. In this analysis, the lower temperature limit was set at 4 K, while the upper temperature limit was systematically varied in 0.5-K increments up to 18 K [see inset of Fig. 2(b)] following the procedure described in Ref. [11]. The estimated temperature-independent fit parameter gives $\mu_{\text{eff}} = 2.51\ \mu_B$, which is much smaller than the $\mu_{\text{eff}} = 4.54\ \mu_B$ resulting from the Hund's rule for a free Yb^{3+} ($J = \frac{7}{2}$) spin. This indicates the formation of a Kramers doublet ground state at low temperatures and $\theta_{\text{CW}} = -0.49 \pm 0.02$ K, which suggests the presence of a weak antiferromagnetic interaction between $J_{\text{eff}} = \frac{1}{2}$ moments of Yb^{3+} ions at low temperature. Based on the effective magnetic moment μ_{eff} value of 2.51, the powder-averaged Landé g factor is found to be 2.89. In the mean-field approximation, the Curie-Weiss temperature θ_{CW} can be expressed as $\theta_{\text{CW}} = (-zJS(S+1))/(3k_B)$, where J represents the exchange interaction between the $J_{\text{eff}} = \frac{1}{2}$ moment of Yb^{3+} ions in the ab plane and z denotes the number of nearest neighbors. In the case of BYTO, where $S = J_{\text{eff}} = \frac{1}{2}$ and $z = 6$, the obtained value of J/k_B is 0.32 K [58]. Another report on BYTO also suggests the existence of weak magnetic interactions between $J_{\text{eff}} = \frac{1}{2}$ moments of Yb^{3+} ions [79].

Figure 2(c) displays the magnetization curve at various temperatures. As corroborated by the specific heat data discussed below, BYTO behaves like a paramagnet above 1 K; therefore one can extract the powder-averaged Landé g factor following the relation $M/M_s = B_{1/2}(y)$, where $B_J(y) = [\frac{2J+1}{2J}\coth(\frac{y(2J+1)}{2J}) - \frac{1}{2J}\coth(\frac{y}{2J})]$ represents the Brillouin function. Here, M is the measured magnetization, $M_s\ (= gJ\mu_B)$ is the saturation magnetization, and $y = g\mu_B J\mu_0 H/k_B T$, with μ_B denoting the Bohr magneton and g representing the Landé g factor. The solid curves in Fig. 2(c) correspond to the fitting of the Brillouin function, yielding an average value of $g = 2.76$, which is close to that estimated from the Curie-Weiss fit of low-temperature susceptibility data.

C. Specific heat

In order to unveil the magnetic ground state influenced by spin frustration and the correlation between Yb^{3+} moments within the Kramers doublet ground state with $J_{\text{eff}} = \frac{1}{2}$ moments in BYTO, it is crucial to conduct experiments at millikelvin temperatures owing to the weak exchange coupling between Yb^{3+} moments. Hence we performed specific heat measurements in a broad range of temperatures and magnetic fields. Figure 3(a) depicts the total specific heat C_{p} data measured in a zero magnetic field down to 49 mK. Below $T \leqslant 3$ K, the specific heat data in zero magnetic field reveal two anomalies, one at 2.22 K and the other at 77 mK, as depicted in the inset of Fig. 3(a). The anomaly at 2.22 K arises from the long-range magnetic ordering due to the presence of an unavoidable minor impurity phase of Yb_2O_3 [70–72]. On the other hand, the anomaly observed at 77 mK is attributed to the long-range magnetic order possibly related to a weak interlayer interaction between Yb^{3+} ions decorated on the triangular lattice.

In BYTO, the total specific heat can be represented as the combination of three components: the magnetic specific heat $C_{\text{mag}}(T)$ originating from magnetic Yb^{3+} ions, the lattice specific heat $C_{\text{lat}}(T)$ attributed to the phonons, and the nuclear specific heat resulting from the nuclear spins of Yb [80]. In order to extract the entropy release resulting from the antiferromagnetic phase transition and the magnetic specific heat, it is necessary to subtract the lattice and nuclear contributions to the total specific heat data. For this purpose, first, the lattice contribution was subtracted following the Debye-Einstein model of lattice specific heat with one Debye term and three Einstein terms, i.e., $C_{\text{lat}}(T) = C_D[9k_B(\frac{T}{\theta_D})^3\int_0^{\theta_D/T}\frac{x^4e^x}{(e^x-1)^2}dx] + \sum_{i=1}^{3} C_{E_i}[3R(\frac{\theta_{E_i}}{T})^2\frac{\exp(\frac{\theta_{E_i}}{T})}{(\exp(\frac{\theta_{E_i}}{T})-1)^2}]$, where θ_D is the Debye temperature, θ_{E_i} are Einstein temperatures, and R and k_B are the molar gas constant and Boltzmann constant, respectively. The good fit, as shown in Fig. 3(a), suggests that the Debye-Einstein model reproduces well the lattice specific heat in this material [81]. The best fit in the temperature range 30 K $\leqslant T \leqslant$ 160 K [see Fig. 3(a)] yielded the values $\theta_D = 179$ K, $\theta_{E_1} = 260$ K, $\theta_{E_2} = 506$ K, and $\theta_{E_3} = 1500$ K [82]. During the fitting procedure, the relative weights of acoustic and optical modes of vibration, i.e., C_D and C_{E_i}, were assigned at a fixed ratio of $C_D : C_{E_1} : C_{E_2} : C_{E_3} = 1 : 2 : 3 : 8.5$, which is consistent with the ratio of the number of heavy atoms (Ba, Yb, Ti) to the number of light atoms (O) in BYTO [29,80].

The olive circles in Fig. 3(b) depict the zero-field specific heat data obtained after subtracting the lattice contribution. The anomaly at $T_{\text{N}} = 77$ mK indicates that BYTO undergoes an antiferromagnetic phase transition at low temperature similar to that found in the triangular lattice $NaBaYb(BO_3)_2$ [53]. The weak upturn in specific heat with decreasing temperature

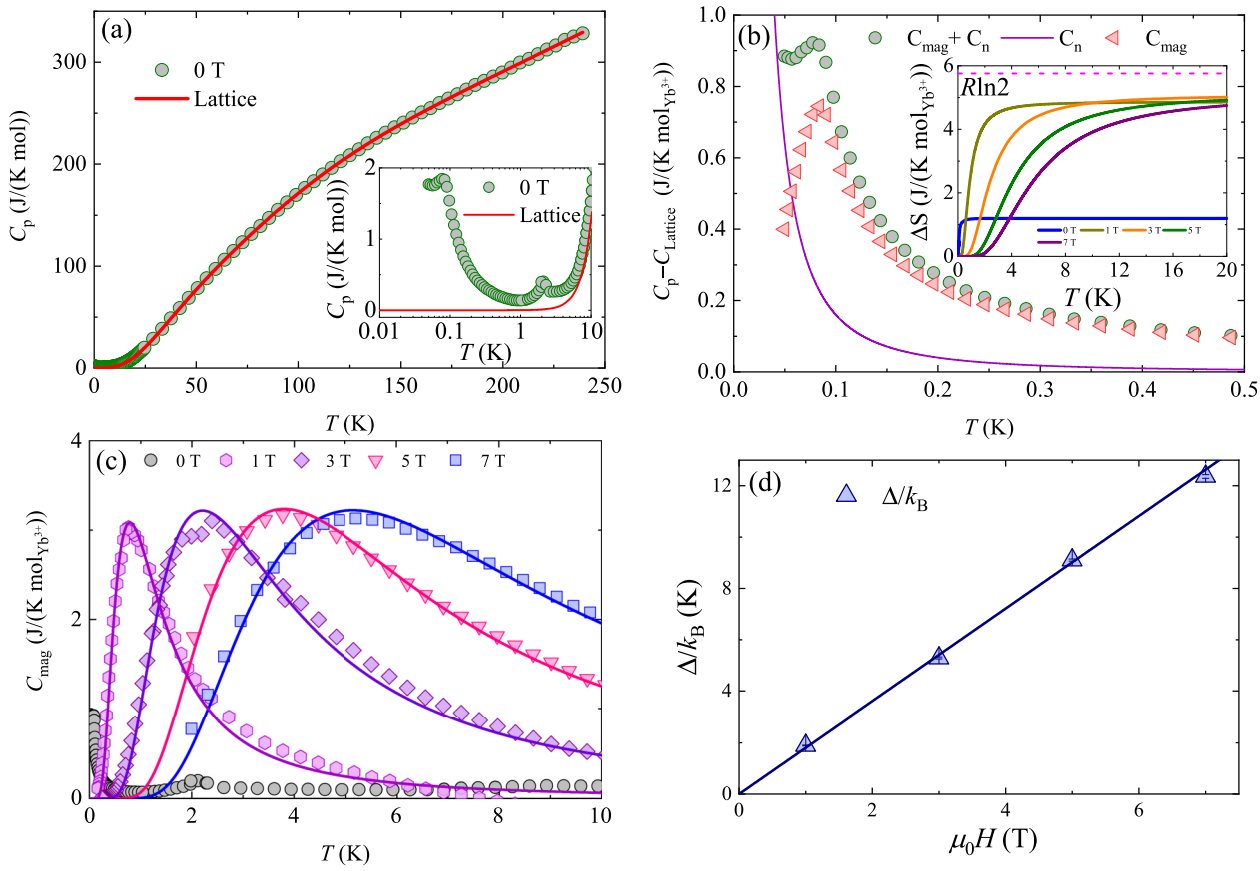

FIG. 3. (a) The temperature dependence of total specific heat C_p of BYTO down to 49 mK in zero magnetic field. The solid curve shows the Debye-Einstein model fit (see text), which represents the phonon specific heat. The inset depicts the appearance of two anomalies upon decreasing the temperature below 3 K. (b) The temperature dependence of specific heat due to the sum of magnetic and nuclear contributions (circles). The triangles represent the intrinsic magnetic specific heat obtained after subtracting nuclear contributions (solid curve). The inset shows the temperature dependence of entropy change up to 20 K in several magnetic fields. The dashed horizontal pink line is the expected entropy for the $J_{\text{eff}} = \frac{1}{2}$ moment. (c) The temperature dependence of the magnetic specific heat in several magnetic fields where the solid curves represent two-level Schottky fit as described in the text. (d) The evolution of a field-induced gap as a function of applied magnetic field, where the solid line represents a linear fit.

($T \leqslant 77$ mK) can be attributed to a nuclear Schottky specific heat owing to the Yb nuclear spins akin to that observed in other Yb-based magnets [53,83]. To account for this contribution, we further subtracted the specific heat due to the nuclear contribution following $C_n \propto 1/T^2$ that is shown by the solid curve in Fig. 3(b) [39]. After subtracting the nuclear Schottky and lattice contributions, the resulting magnetic specific heat data (represented by triangles) are displayed in Fig. 3(b) as a function of temperature in zero magnetic field. Below 1 K, there is a noticeable increase in magnetic specific heat, followed by a sharp anomaly at 77 mK. This strongly suggests the presence of antiferromagnetic long-range order in BYTO. The occurrence of this anomaly at very low temperatures is in agreement with the presence of a weak exchange interaction between Yb^{3+} moments.

The inset in Fig. 3(b) shows the temperature-dependent magnetic entropy change, denoted as $\Delta S(T)$, which is calculated as the integral of $C_{\text{mag}}(T)/T\,dT$ in several magnetic fields. In zero field, below the lowest measured temperature, the magnetic specific heat was obtained using linear interpolation down to zero temperature. Notably, it is observed that the entropy tends to attain a plateau at a value of 1.20 J/(K mol$_{Yb^{3+}}$). This value corresponds to approximately 20% of the expected entropy value of $R\ln 2$ [equal to 5.76 J/(K mol$_{Yb^{3+}}$)] for Yb^{3+} spins with $J_{\text{eff}} = \frac{1}{2}$ moments. The missing 80% entropy can be due to the presence of short-range spin correlations [52,53,84]. The overestimation of the lattice contribution to the missing entropy can be ignored as the experimental temperature range is sufficient to adequately consider the impact of lattice contributions. Furthermore, below the transition temperature T_N, the change in entropy amounts to approximately 5% of $R\ln 2$. This observation implies the existence of substantial magnetic entropy below T_N, likely attributable to significant spin fluctuations with a small ordered moment [85]. Furthermore, the spin fluctuation associated with short-range spin correlations above the transition temperature is also evident from the μSR experiments as discussed in the next section. A common scenario of missing 80% entropy is also observed in the recently reported triangular lattice antiferromagnet $Ba_3Yb(BO_3)_3$ [52]. Nonetheless, the significant entropy retained at temperatures approaching absolute zero may arise from strong quantum fluctuations similar to the one observed in the long-range ordered triangular lattice antiferromagnet $KBaGd(BO_3)_2$ [60,86]. Magnetic entropy tends to

reach 5.76 J/(K $\text{mol}_{\text{Yb}^{3+}}$) in high magnetic fields, indicating the presence of $J_{\text{eff}} = \frac{1}{2}$ moments.

In order to investigate the effect of magnetic field on the antiferromagnetically ordered ground state of BYTO, specific heat measurements were performed in different magnetic fields. After subtracting the lattice contributions, the obtained magnetic specific heat in different magnetic fields is shown in Fig. 3(c). It is observed that the anomaly at 77 mK disappears when a magnetic field of $\mu_0 H = 1$ T is applied. This is a common feature observed in certain rare-earth magnets, including the material under investigation, where a strong magnetic field suppresses the exchange interactions. In such a scenario, the external magnetic field induces the Zeeman splitting of the lowest Kramers doublet state. Consequently, a Schottky-like broad peak emerges in the specific heat as depicted in Fig. 3(c). Furthermore, it is worth noting that as the strength of the applied magnetic field increases, the broad peak shifts towards higher temperatures, similar to the shift observed in several other rare-earth magnets [28,53].

To deduce the gap induced by the Zeeman splitting of the lowest Kramers doublet due to the applied magnetic field, we employed the simplest two-level Schottky specific heat model [82], i.e.,

$$C_{\text{Sch}} = fR\left(\frac{\Delta}{k_B T}\right)^2 \frac{\exp(\Delta/k_B T)}{(1+\exp(\Delta/k_B T))^2}, \qquad (1)$$

where Δ is the Zeeman splitting of the ground-state Kramers doublet of Yb^{3+} ions, k_B is the Boltzmann constant, R is the universal gas constant, and f measures the fraction of Yb^{3+} spins which contributes to the splitting of the ground-state doublet. In Fig. 3(c), the solid curves illustrate that the two-level Schottky fit effectively describes the magnetic specific heat data acquired in several magnetic fields. Notably, the estimated Zeeman gap Δ is observed to exhibit a linear variation with the external magnetic field, as depicted in Fig. 3(d). A similar linear variation of Δ, derived from inelastic neutron scattering experiments performed in a magnetic field, has also been observed for polycrystalline samples of BYTO [79]. From a linear fit we find the value of the Landé g factor, estimated to be $g = 2.66 \pm 0.02$, which is close to that determined from the magnetization data. Moreover, the Schottky fit yields a value of approximately $f \sim 0.9$ for nonzero magnetic fields. This indicates that nearly all of the Yb^{3+} spins are involved in contributing to the Schottky specific heat in magnetic fields.

D. Thermal conductivity

Thermal conductivity is a very sensitive probe to identify low-energy excitations which can carry heat or scatter heat carriers at low temperature in correlated quantum materials. Since the specific heat data are dominated by nuclear Schottky and lattice contributions, thermal conductivity is highly advantageous to probe the nature of ground-state excitations, whether it is gapped or gapless. Figure 4 depicts the temperature dependence of the thermal conductivity κ of a polycrystalline sample of BYTO. With decreasing temperature a well-defined broad peak appears around 20 K, which can be understood as the so-called phonon peak [87–89]. The appearance of such a peak is expected for typical insulating

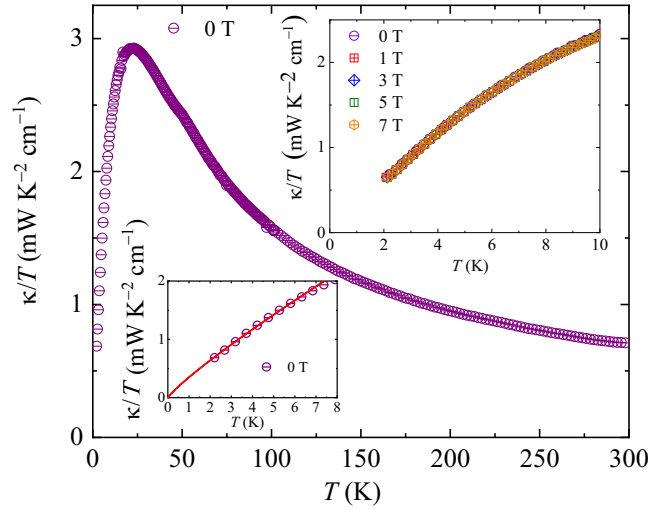

FIG. 4. The temperature dependence of thermal conductivity divided by temperature (κ/T) of BYTO in zero magnetic field. The top left inset shows κ/T vs temperature in different magnetic fields up to 7 T. The bottom right inset displays κ/T vs temperature in zero field, where the red curve represents the fit with a phenomenological model as described in the text.

behavior of good-quality polycrystalline samples. As depicted in the top right inset of Fig. 4, there is no effect of magnetic field on thermal conductivity, which implies that up to 2 K thermal conductivity is entirely dominated by phonons. Given that the interaction energy scale is approximately 0.30 K, magnetic excitations may potentially contribute to thermal conductivity at subkelvin temperatures. For some insulating materials, thermal conductivity at low temperature can be described as $\kappa/T = a + b\,T^{\alpha-1}$, where the first term represents the contribution of itinerant low-energy magnetic excitations and the second term is due to the contribution of phonons where the value of α typically lies in the range $2 \leqslant \alpha \leqslant 3$ due to scattering of phonons from sample boundaries of a clean single crystal [90,91]. The low-temperature κ/T data were fitted by $\kappa/T = b\,T^{\alpha-1}$ as shown in the bottom left inset of Fig. 4. The obtained value for α was found to be 1.87 ± 0.05, which is close to the expected value for polycrystalline samples [92]. For the triangular lattice antiferromagnets $NaYbSe_2$ and $YbMgGaO_4$, a similar value of α is also observed at lower temperature ($T \ll |\theta_{\text{CW}}|$) [93,94]. The measured temperature range is not sufficiently low to observe the contribution from magnetic excitations, which invokes future studies to shed more light on the ground-state properties of this frustrated magnet.

E. Muon spin relaxation

In order to gain microscopic insights into the ground-state properties and spin dynamics, we performed highly sensitive muon spin relaxation measurements down to a base temperature of 80 mK. Figure 5 depicts the zero-field (ZF) and longitudinal field (LF) μSR data, showing their evolution at several temperatures for BYTO. As shown in Fig. 5(a), the ZF-μSR spectra exhibit no indications of either an oscillating component or a "$\frac{1}{3}$" tail that reflects the lack of internal static

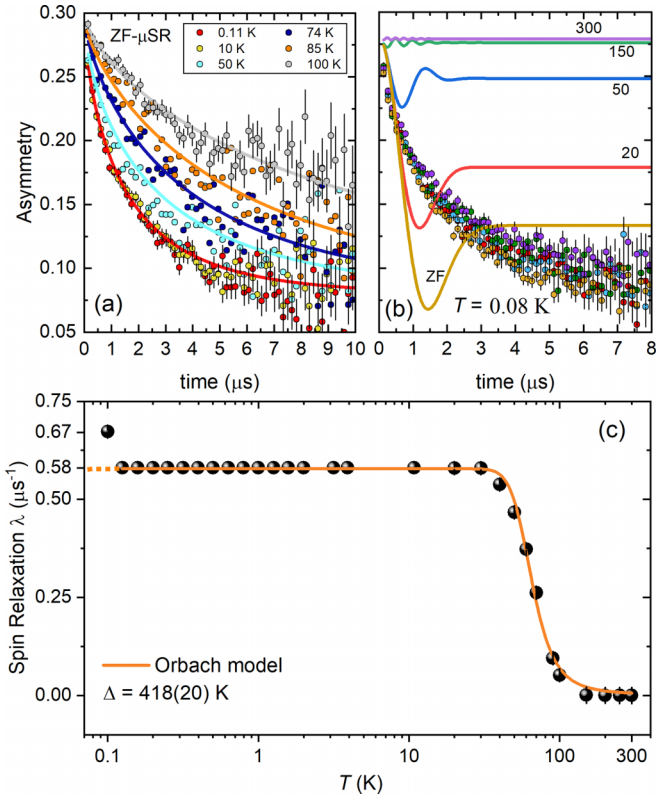

FIG. 5. (a) Evolution in temperature of the zero-field asymmetry as a function of time for BYTO. Curves are fits with a stretched exponential. (b) Evolution of the asymmetry under applied longitudinal fields (circles from ZF to 300 Oe) and comparison with the behavior of the static Kubo-Toyabe function for corresponding magnetic fields (curves, in oersteds), highlighting the dynamical behavior of Yb^{3+} moments at 0.08 K. (c) Temperature dependence of the muon spin relaxation rate λ extracted from fits to the data shown in (a).

magnetic fields down to 0.11 K. Nevertheless, the transition to magnetic ordering may not always be defined by oscillations in the ZF muon spin asymmetry; instead it can manifest as modifications in the asymmetry line shape [95]. These are not observed in BYTO either as all the ZF spectra are well fitted with a stretched exponential function, $A(t) = \exp[-(\lambda t)^{\beta}] + B$, with a moderate $\beta \simeq 0.8(1)$ and a background constant term B. The stretching parameter β is found to be temperature independent and thus likely accounts for multiple relaxation rates due to a nonunique muon stopping site in the crystal structure. Upon cooling, the spin relaxation rate λ reaches a plateau at a value of 0.58(3) μs^{-1} below 10 K and down to 0.125 K. We noticed a slight increase in the muon spin relaxation rate at 100 mK, perhaps indicative of a crossover towards a more correlated regime, as pointed out by the anomaly found at 77 mK in specific heat. The slowing down of spin fluctuations observed between 300 and 30 K occurs in a typical temperature range of crystal electric field levels of Yb^{3+} [96], to which the muon is sensitive through the Orbach process, with a muon spin relaxation rate modeled by [11,97]

$$\lambda = \left(C e^{-\Delta/k_B T} + \frac{1}{\lambda_0} \right)^{-1} \qquad (2)$$

with $\lambda_0 = 0.58(3)\ \mu s^{-1}$ being the relaxation rate when $T \to 0$, C being an amplitude parameter, and $\Delta = 418(20)$ K being the gap to the first excited crystal field level. The large value of Δ ensures that only the Kramers ground-state doublet is occupied at low temperature and that it is well separated from the excited states, which confirms the validity of the $J_{\text{eff}} = \frac{1}{2}$ picture in BYTO.

In addition, a series of LF measurements were performed at 80 mK [Fig. 5(b)] to gain insight into the dynamics of the electronic magnetic moment. For large values of LF, in comparison with any static magnetic fields, the motion of muon spins is determined by the LF only, and the asymmetry becomes nearly constant. Consequently, any remaining depolarization of the muon spin is attributed to fluctuations due to electronic magnetic moments when the LF overcomes local static fields, if there are any. As shown in Fig. 5(b), even for large applied fields, the relaxation remains exponential. A crude comparison with a simple static Kubo-Toyabe relaxation form clearly fails to reproduce the data and demonstrates the dynamical nature of the Yb^{3+} moments at this temperature. A fluctuating regime is thus observed from 10 K down to 0.1 K with no slowing down below ∼4 K, in contrast to the related $J_{\text{eff}} = \frac{1}{2}$ Yb triangular quantum spin-liquid candidate $YbMgGaO_4$ [34] but in agreement with the lower energy scale of the interaction in BYTO.

F. Electron spin resonance

To study the nature of dominant magnetic interaction between Yb^{3+} spins in BYTO, we performed ESR measurements on polycrystalline samples of BYTO. The ESR spectra contain a broad main component centered around $B_0 = 5.8$ T and a secondary narrow component centered at 7.54 T [Fig. 6(a)]. At 5 K the intensity of the secondary component amounts to only 0.4% of the main one and is therefore attributed to a minor impurity phase. The main ESR line is composed of several pronounced features due to the polycrystalline nature of our sample. A simulation of the powder-averaged spectrum works well with Lorentzian line shape and three independent g-factor components and linewidths [simulation 1 in Fig. 6(b)], which is compatible with the distortion of the YbO_6 octahedra away from cubic symmetry. At 5 K, we find the g-factor eigenvalues $g_x = 2.38$, $g_y = 2.80$, and $g_z = 3.78$ and the corresponding linewidths $\Delta B_x = 1.0$ T, $\Delta B_y = 0.9$ T, and $\Delta B_z = 2.5$ T. The fit is considerably worse if only two independent g factors and linewidths are considered [simulation 2 in Fig. 6(b)]. The latter model assuming axial symmetry around the crystallographic c axis would apply for strongly exchange-coupled Yb^{3+} moments on the unit triangle [98].

The fact that the ESR spectrum does not obey the uniaxial symmetry of the underlying spin lattice limits the isotropic intratrimer exchange interactions that would lead to exchange narrowing with $J \ll \mu_B \Delta g B_0 / k_B \simeq 6$ K, where μ_B and k_B are the Bohr magneton and the Boltzmann constant, respectively, and $\Delta g = g_z - g_x = 1.4$ denotes the spread of the g factor at 5 K. The detected ESR linewidth is extremely broad and cannot be accounted for by simple dipolar interactions between Yb^{3+} moments, which would result in an ESR linewidth of the order of $\mu_0 \mu / (4\pi r^3) = 11$ mT, where μ_0 is the vacuum

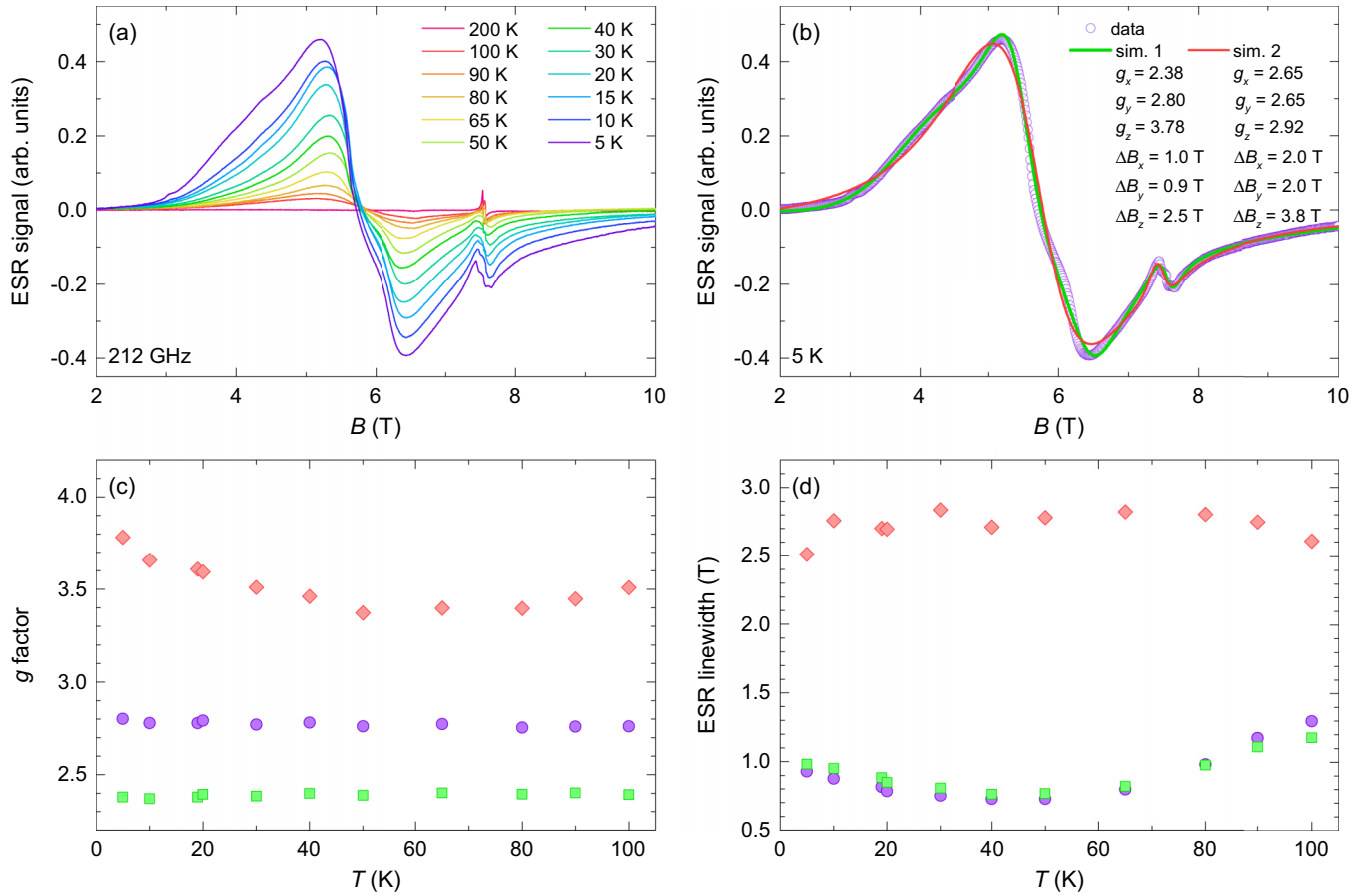

FIG. 6. (a) The temperature evolution of the ESR spectra of BYTO. (b) Fit of the ESR spectrum at 5 K (points) with a powder-averaged Lorentzian line shape with three independent g factors [simulation (sim.) 1] and two independent g factors (simulation 2), the latter assuming uniaxial symmetry of the crystal lattice. (c) The temperature dependence of the three g-factor eigenvalues and (d) ESR linewidths for simulation 1.

permeability, $\mu = 2.51\mu_B$ is the Yb^{3+} magnetic moment in the ground state, and $r = 5.91$ Å is the nearest-neighbor distance. Therefore much larger magnetic anisotropy resulting from exchange interactions must also be present. When the anisotropic exchange D dominates over the isotropic exchange, as regularly encountered for rare-earth ions [11], the ESR linewidth ΔB is given by $g\mu_B\Delta B \sim k_B D$ [99]. This yields an anisotropy of the order of a few kelvins in BYTO. With increasing temperature the intensity of the ESR signal decreases profoundly [Fig. 6(a)], following a Curie-like dependence, which is in agreement with small exchange interactions. The fit of the ESR spectrum becomes unreliable above 100 K, and the spectrum is completely lost at 200 K. We find that the ESR linewidths [Fig. 6(d)] and g factors [Fig. 6(c)], however, only slightly change with temperature, in agreement with the observation that the ground-state Kramers doublet is well separated from excited Kramers doublets. Furthermore, phonon-related ESR broadening mechanisms, which are all characterized by profound temperature dependence [99], must be negligible in this temperature range.

IV. DISCUSSION

In rare-earth magnets, the electronic state of the rare-earth ion is mostly governed by the crystalline electric field at the rare-earth site and the number of electrons in the $4f$ shell. Depending on this electronic state, the crystalline anisotropy, and the presence of a favorable exchange path, rare-earth magnets can host distinct ground-state properties [31]. In rare-earth magnets with an odd number of $4f$ electrons, the crystal electric field usually splits the magnetic ground state of a free rare-earth ion into Kramers doublets, where $4f$ ions acquire pseudospin $J_{\text{eff}} = \frac{1}{2}$ moments in the ground-state doublet that are protected by time-reversal symmetry [43].

In the present antiferromagnet, BYTO (Yb^{3+}, $4f^{13}$), the crystalline electric field generated by nearby O^{2-} ions can split the $2J + 1 = 8$ degenerate ground state ($^2F_{7/2}$) into four Kramers doublets. The presence of these low-energy Kramers doublet states in BYTO has been indicated already through magnetic susceptibility measurements. At low temperatures, the magnetic susceptibility data follow a Curie-Weiss law with effective moment $\mu_{\text{eff}} = 2.51\ \mu_B$ that is much less than the effective moment of free Yb^{3+} ions, which suggests the formation of a Kramers doublet state with spin-orbit driven $J_{\text{eff}} = \frac{1}{2}$ moment of Yb^{3+} ions. The estimated negative θ_{CW} value, $\theta_{\text{CW}} = -0.49$ K, from low-temperature susceptibility data indicates the presence of antiferromagnetic interaction though the strength of interaction is weak but typical of $4f$ magnets [29]. The zero-field specific heat data clearly show an anomaly at $T_{\text{N}} = 77$ mK, which is tentatively assigned

to antiferromagnetic long-range magnetic order in BYTO. Nonetheless, the anomaly occurring at T_N vanishes when subjected to a magnetic field with $\mu_0 H \geqslant 1$ T, and instead, a broad maximum emerges at higher temperatures. This scenario is a common occurrence in rare-earth magnets, where the influence of Zeeman splitting resulting from an external magnetic field surpasses the weak exchange interactions between rare-earth moments, leading the system towards a field-polarized state [53,60]. As the magnetic field strength increases, the observed broad peak in specific heat for $\mu_0 H \geqslant 1$ T broadens and shifts towards higher temperatures. This reflects the Zeeman splitting of the lowest Kramers doublet state of BYTO, a phenomenon commonly observed in rare-earth magnets [28,72,79]. The obtained 20% entropy in zero magnetic field is less than the expected entropy ($R \ln 2$) for $J_{\text{eff}} = \frac{1}{2}$, suggesting there could be two origins of missing entropy: One is spin fluctuations in the ordered state, and the other is the presence of short-range spin correlations above the transition temperature due to moderate spin frustration defined by $f = |\theta_{\text{CW}}|/T_N \approx 6$ [53,84].

In the literature there are several reports on Yb-based triangular lattice antiferromagnets where the exchange interaction between rare-earth moments is found to be the sum of dipolar and superexchange interactions [60,100]. The intraplane Yb-Yb distance in BYTO is almost double that of the intra-planar distance in YbMgGaO4, which suggests the presence of weak magnetic dipole-dipole interaction, approximately 0.017 K as estimated using $E_{\text{dip}} \approx \mu_0 g_{\text{av}}^2 \mu_B^2 / 4\pi a^3$, where g_{av} is the powder-averaged Landé g factor and a is the nearest-neighbor Yb-Yb distance in BYTO. The obtained dipolar interaction is only 5% of the nearest-neighbor exchange interaction as estimated from the Curie-Weiss temperature following the mean-field approximation. This suggests the presence of dominant superexchange interaction between the $J_{\text{eff}} = \frac{1}{2}$ moments of Yb^{3+} ions. Our ESR results also indicate, apart from dipolar interaction, the presence of finite exchange interactions in BYTO, which, however, is anisotropic. In BYTO, YbO_6 octahedra are isolated instead of being corner- and side-sharing regular octahedra as observed in $YbMgGaO_4$. Thus, in BYTO, the nearest-neighbor intraplane superexchange interaction can only be possible via the f-p-d-p-f (Yb-O-Ti-O-Yb) virtual path, which is likely one of the reasons for the weak antiferromagnetic interaction strength in BYTO. In contrast, in $YbMgGaO_4$, the nearest-neighbor superexchange interaction is directly mediated by the oxygen ion via the f-p-f (Yb-O-Yb) virtual electron hopping processes, and as a result, the antiferromagnetic interaction in $YbMgGaO_4$ is a bit stronger (≈ 2 K) [101]. From crystallographic parameters, it is observed that the interplanar distance in BYTO is approximately 7.26 Å and is slightly larger than the nearest-neighbor distance ($\sim$5.92 Å) between rare-earth moments. Furthermore, in the triangular planes, the bond distance of the second-nearest neighbor of the Yb^{3+} ion is roughly 10.23 Å, which is larger than the interplanar separation, causing there to be significant exchange coupling in BYTO. Therefore it is most likely that in addition to intraplane nearest-neighbor exchange interactions, the presence of non-negligible interplane exchange interactions through the Ti_2O_9 dimer leads to long-range magnetic order in this triangular lattice antiferromagnet. An antiferromagnetic phase transition due to interlayer interaction is also observed in the triangular lattice antiferromagnet $Ba_3CoSb_2O_9$ (Co^{2+}; $J_{\text{eff}} = \frac{1}{2}$), which has similar crystallographic symmetry, intralayer and interlayer exchange paths, and interlayer distance to those of BYTO [76,102].

The μSR experiments reveal a fluctuating state of Yb^{3+} moments in the temperature range 0.1 K $\leqslant T \leqslant$ 10 K and do not show any signature of long-range magnetic order down to 80 mK. The broadening of the ESR spectrum at 5 K indicates the presence of anisotropy in the exchange interaction between the Yb^{3+} spins; otherwise one would observe a narrow ESR spectrum for isotropic exchange interaction [103]. We also found large g-factor anisotropy, which is compatible with the distortion of the YbO_6 octahedra from cubic symmetry. The temperature-independent g factor in the broad temperature range implies a well-separated lowest Kramers doublet state, which is consistent with the μSR results. The estimated g value from the ESR spectrum at 5 K leads to the powder-averaged value $g = \sqrt{(g_x^2 + g_y^2 + g_z^2)/3} = 3.04$, which is close to that obtained from magnetization data. Theoretically, it is predicted that apart from interlayer exchange interaction, the nearest-neighbor exchange interaction with either easy-plane or easy-axis anisotropy can lead to a long-range ordered state in rare-earth-based triangular lattice antiferromagnets [31]. The role of anisotropic exchange interaction in stabilizing the long-range ordered state is not yet clear from the present study and will be a subject of detailed future investigations.

V. CONCLUSION

We have presented the synthesis, crystal structure, thermodynamic, muon spin relaxation, and electron spin resonance results of the triangular lattice antiferromagnet $Ba_6Yb_2Ti_4O_{17}$, which crystallizes in a highly symmetric crystal structure with space group $P6_3/mmc$ without any detectable antisite disorder between atomic sites. The present compound constitutes close-to-structurally-perfect two-dimensional triangular layers of Yb^{3+} ions perpendicular to the crystallographic c axis. The magnetic susceptibility and electron spin resonance measurements suggest the presence of weak antiferromagnetic interaction between $J_{\text{eff}} = \frac{1}{2}$ moments of Yb^{3+} ions. The anomaly observed at $T_N = 77$ mK in the zero-field specific heat data is attributed to the presence of long-range magnetic order which vanishes in magnetic field $\mu_0 H \geqslant 1$ T. Furthermore, the specific heat data suggest the presence of a field-induced gap due to Zeeman splitting of the Kramers doublet ground state in a weak magnetic field. The μSR experiments reveal a fluctuating regime in 0.1 K $\leqslant T \leqslant$ 10 K ascribed to the depopulation of crystal electric field levels, in agreement with a well-separated Kramers doublet, and the enhancement of the muon spin relaxation rate below 100 mK might be associated with a more correlated regime of Yb^{3+} moments that is consistent with the presence of an anomaly in specific heat. Our ESR results further confirm that the lowest Kramers doublet is well separated from the excited doublet state and point to the presence of anisotropic exchange interaction between Yb^{3+} spins in the present antiferromagnet. Despite the moderate spin frustration, a combination of exchange anisotropy and interlayer magnetic interaction are

most likely stabilize long-range magnetically ordered state in $Ba_6Yb_2Ti_4O_{17}$. Future experiments may provide detailed insights into the microscopic Hamiltonian and the precise nature of magnetic anisotropy and spin correlations in this class of spin-orbit driven $J_{\text{eff}} = \frac{1}{2}$ triangular lattice antiferromagnets.

ACKNOWLEDGMENTS

P.K. acknowledges funding by the Science and Engineering Research Board and Department of Science and Technology, India, through research grants. A.Z. acknowledges the financial support of the Slovenian Research and Innovation Agency through Program No. P1-0125 and Projects No. J1-50008 and No. BI-US/22-24-065. E.K. acknowledges financial support from Labex PALM for the QuantumPyroMan project (Project No. ANR-10-LABX-0039-PALM). A.M.S. thanks the URC/FRC of UJ and South Africa's National Research Foundation (Grant No. 93549) for financial support. A portion of this work was performed at the National High Magnetic Field Laboratory, which is supported by the National Science Foundation Cooperative Agreement No. DMR-2128556* and the State of Florida.

[1] L. Balents, Nature (London) **464**, 199 (2010).
[2] T. Oka and S. Kitamura, Annu. Rev. Condens. Matter Phys. **10**, 387 (2019).
[3] B. Keimer and J. E. Moore, Nat. Phys. **13**, 1045 (2017).
[4] W. Witczak-Krempa, G. Chen, Y. B. Kim, and L. Balents, Annu. Rev. Condens. Matter Phys. **5**, 57 (2014).
[5] J. K. Glasbrenner, I. I. Mazin, H. O. Jeschke, P. J. Hirschfeld, R. M. Fernandes, and R. Valentí, Nat. Phys. **11**, 953 (2015).
[6] J. Khatua, B. Sana, A. Zorko, M. Gomilšek, K. Sethupathi, M. R. Rao, M. Baenitz, B. Schmidt, and P. Khuntia, Phys. Rep. **1041**, 1 (2023).
[7] L. Savary and L. Balents, Rep. Prog. Phys. **80**, 016502 (2017).
[8] C. Broholm, R. J. Cava, S. A. Kivelson, D. G. Nocera, M. R. Norman, and T. Senthil, Science **367**, eaay0668 (2020).
[9] P. Anderson, Mater. Res. Bull. **8**, 153 (1973).
[10] M. Klanjšek, A. Zorko, R. Žitko, J. Mravlje, Z. Jagličić, P. K. Biswas, P. Prelovšek, D. Mihailovic, and D. Arčon, Nat. Phys. **13**, 1130 (2017).
[11] T. Arh, B. Sana, M. Pregelj, P. Khuntia, Z. Jagličić, M. D. Le, P. K. Biswas, P. Manuel, L. Mangin-Thro, A. Ozarowski, and A. Zorko, Nat. Mater. **21**, 416 (2022).
[12] P. Khuntia, R. Kumar, A. V. Mahajan, M. Baenitz, and Y. Furukawa, Phys. Rev. B **93**, 140408(R) (2016).
[13] Y. Shimizu, K. Miyagawa, K. Kanoda, M. Maesato, and G. Saito, Phys. Rev. Lett. **91**, 107001 (2003).
[14] S. Yunoki and S. Sorella, Phys. Rev. B **74**, 014408 (2006).
[15] P. A. Maksimov, Z. Zhu, S. R. White, and A. L. Chernyshev, Phys. Rev. X **9**, 021017 (2019).
[16] Y. Zhou, K. Kanoda, and T.-K. Ng, Rev. Mod. Phys. **89**, 025003 (2017).
[17] C. Nayak, S. H. Simon, A. Stern, M. Freedman, and S. Das Sarma, Rev. Mod. Phys. **80**, 1083 (2008).
[18] A. Kitaev, Ann. Phys. (Amsterdam) **321**, 2 (2006).
[19] P. Khuntia, J. Magn. Magn. Mater. **489**, 165435 (2019).
[20] T.-H. Han, J. S. Helton, S. Chu, D. G. Nocera, J. A. Rodriguez-Rivera, C. Broholm, and Y. S. Lee, Nature (London) **492**, 406 (2012).
[21] R. Dally, T. Hogan, A. Amato, H. Luetkens, C. Baines, J. Rodriguez-Rivera, M. J. Graf, and S. D. Wilson, Phys. Rev. Lett. **113**, 247601 (2014).
[22] P. Khuntia, F. Bert, P. Mendels, B. Koteswararao, A. V. Mahajan, M. Baenitz, F. C. Chou, C. Baines, A. Amato, and Y. Furukawa, Phys. Rev. Lett. **116**, 107203 (2016).
[23] B. Gao, T. Chen, D. W. Tam, C.-L. Huang, K. Sasmal, D. T. Adroja, F. Ye, H. Cao, G. Sala, M. B. Stone, C. Baines, J. A. T. Verezhak, H. Hu, J.-H. Chung, X. Xu, S.-W. Cheong, M. Nallaiyan, S. Spagna, M. B. Maple, A. H. Nevidomskyy *et al.* Nat. Phys. **15**, 1052 (2019).
[24] L. Savary and L. Balents, Phys. Rev. Lett. **118**, 087203 (2017).
[25] J. Khatua, M. Gomilšek, J. C. Orain, A. M. Strydom, Z. Jagličić, C. V. Colin, S. Petit, A. Ozarowski, L. Mangin-Thro, K. Sethupathi, M. S. R. Rao, A. Zorko, and P. Khuntia, Commun. Phys. **5**, 99 (2022).
[26] L. T. Nguyen, D. B. Straus, Q. Zhang, and R. J. Cava, Phys. Rev. Mater. **5**, 034419 (2021).
[27] Y. Li, Adv. Quantum Technol. **2**, 1900089 (2019).
[28] J. Khatua, S. Bhattacharya, Q. P. Ding, S. Vrtnik, A. M. Strydom, N. P. Butch, H. Luetkens, E. Kermarrec, M. S. R. Rao, A. Zorko, Y. Furukawa, and P. Khuntia, Phys. Rev. B **106**, 104404 (2022).
[29] J. Khatua, M. Pregelj, A. Elghandour, Z. Jagličic, R. Klingeler, A. Zorko, and P. Khuntia, Phys. Rev. B **106**, 104408 (2022).
[30] E. M. Smith, O. Benton, D. R. Yahne, B. Placke, R. Schäfer, J. Gaudet, J. Dudemaine, A. Fitterman, J. Beare, A. R. Wildes, S. Bhattacharya, T. DeLazzer, C. R. C. Buhariwalla, N. P. Butch, R. Movshovich, J. D. Garrett, C. A. Marjerrison, J. P. Clancy, E. Kermarrec, G. M. Luke *et al.*, Phys. Rev. X **12**, 021015 (2022).
[31] Z. Zhu, P. A. Maksimov, S. R. White, and A. L. Chernyshev, Phys. Rev. Lett. **120**, 207203 (2018).
[32] B. Bernu, P. Lecheminant, C. Lhuillier, and L. Pierre, Phys. Rev. B **50**, 10048 (1994).
[33] Y. Li, H. Liao, Z. Zhang, S. Li, F. Jin, L. Ling, L. Zhang, Y. Zou, L. Pi, Z. Yang, J. Wang, Z. Wu, and Q. Zhang, Sci. Rep. **5**, 16419 (2015).
[34] Y. Li, D. Adroja, P. K. Biswas, P. J. Baker, Q. Zhang, J. Liu, A. A. Tsirlin, P. Gegenwart, and Q. Zhang, Phys. Rev. Lett. **117**, 097201 (2016).
[35] Y. Shen, Y.-D. Li, H. Wo, Y. Li, S. Shen, B. Pan, Q. Wang, H. C. Walker, P. Steffens, M. Boehm, Y. Hao, D. L. Quintero-Castro, L. W. Harriger, M. D. Frontzek, L. Hao, S. Meng, Q. Zhang, G. Chen, and J. Zhao, Nature (London) **540**, 559 (2016).
[36] W. Liu, Z. Zhang, J. Ji, Y. Liu, J. Li, X. Wang, H. Lei, G. Chen, and Q. Zhang, Chin. Phys. Lett. **35**, 117501 (2018).
[37] J. Xing, L. D. Sanjeewa, J. Kim, G. R. Stewart, A. Podlesnyak, and A. S. Sefat, Phys. Rev. B **100**, 220407(R) (2019).
[38] M. Baenitz, P. Schlender, J. Sichelschmidt, Y. A. Onykiienko, Z. Zangeneh, K. M. Ranjith, R. Sarkar, L. Hozoi, H. C. Walker,

J.-C. Orain, H. Yasuoka, J. van den Brink, H. H. Klauss, D. S. Inosov, and T. Doert, Phys. Rev. B **98**, 220409(R) (2018).
[39] K. M. Ranjith, S. Luther, T. Reimann, B. Schmidt, P. Schlender, J. Sichelschmidt, H. Yasuoka, A. M. Strydom, Y. Skourski, J. Wosnitza, H. Kühne, T. Doert, and M. Baenitz, Phys. Rev. B **100**, 224417 (2019).
[40] M. M. Bordelon, E. Kenney, C. Liu, T. Hogan, L. Posthuma, M. Kavand, Y. Lyu, M. Sherwin, N. P. Butch, C. Brown, M. J. Graf, L. Balents, and S. D. Wilson, Nat. Phys. **15**, 1058 (2019).
[41] L. Ding, P. Manuel, S. Bachus, F. Grußler, P. Gegenwart, J. Singleton, R. D. Johnson, H. C. Walker, D. T. Adroja, A. D. Hillier, and A. A. Tsirlin, Phys. Rev. B **100**, 144432 (2019).
[42] R. Sarkar, P. Schlender, V. Grinenko, E. Haeussler, P. J. Baker, T. Doert, and H.-H. Klauss, Phys. Rev. B **100**, 241116(R) (2019).
[43] P.-L. Dai, G. Zhang, Y. Xie, C. Duan, Y. Gao, Z. Zhu, E. Feng, Z. Tao, C.-L. Huang, H. Cao, A. Podlesnyak, G. E. Granroth, M. S. Everett, J. C. Neuefeind, D. Voneshen, S. Wang, G. Tan, E. Morosan, X. Wang, H.-Q. Lin *et al.*, Phys. Rev. X **11**, 021044 (2021).
[44] Z. Ma, J. Wang, Z.-Y. Dong, J. Zhang, S. Li, S.-H. Zheng, Y. Yu, W. Wang, L. Che, K. Ran, S. Bao, Z. Cai, P. Čermák, A. Schneidewind, S. Yano, J. S. Gardner, X. Lu, S.-L. Yu, J.-M. Liu, S. Li *et al.*, Phys. Rev. Lett. **120**, 087201 (2018).
[45] I. Kimchi, A. Nahum, and T. Senthil, Phys. Rev. X **8**, 031028 (2018).
[46] G. H. Wannier, Phys. Rev. **79**, 357 (1950).
[47] M. Ulaga, J. Kokalj, A. Wietek, A. Zorko, and P. Prelovšek, Phys. Rev. B **109**, 035110 (2024).
[48] N. Y. Yao, M. P. Zaletel, D. M. Stamper-Kurn, and A. Vishwanath, Nat. Phys. **14**, 405 (2018).
[49] A. M. Hallas, J. Gaudet, and B. D. Gaulin, Annu. Rev. Condens. Matter Phys. **9**, 105 (2018).
[50] C. Y. Jiang, Y. X. Yang, Y. X. Gao, Z. T. Wan, Z. H. Zhu, T. Shiroka, C. S. Chen, Q. Wu, X. Li, J. C. Jiao, K. W. Chen, Y. Bao, Z. M. Tian, and L. Shu, Phys. Rev. B **106**, 014409 (2022).
[51] K. Y. Zeng, L. Ma, Y. X. Gao, Z. M. Tian, L. S. Ling, and L. Pi, Phys. Rev. B **102**, 045149 (2020).
[52] R. Bag, M. Ennis, C. Liu, S. E. Dissanayake, Z. Shi, J. Liu, L. Balents, and S. Haravifard, Phys. Rev. B **104**, L220403 (2021).
[53] S. Guo, A. Ghasemi, C. L. Broholm, and R. J. Cava, Phys. Rev. Mater. **3**, 094404 (2019).
[54] B. L. Pan, J. M. Ni, L. P. He, Y. J. Yu, Y. Xu, and S. Y. Li, Phys. Rev. B **103**, 104412 (2021).
[55] J. M. Kosterlitz and D. J. Thouless, J. Phys. C: Solid State Phys. **6**, 1181 (1973).
[56] Y. Gao, Y.-C. Fan, H. Li, F. Yang, X.-T. Zeng, X.-L. Sheng, R. Zhong, Y. Qi, Y. Wan, and W. Li, npj Quantum Mater. **7**, 89 (2022).
[57] Z. Hu, Z. Ma, Y.-D. Liao, H. Li, C. Ma, Y. Cui, Y. Shangguan, Z. Huang, Y. Qi, W. Li, Z. Y. Meng, J. Wen, and W. Yu, Nat. Commun. **11**, 5631 (2020).
[58] H. Li, Y. D. Liao, B.-B. Chen, X.-T. Zeng, X.-L. Sheng, Y. Qi, Z. Y. Meng, and W. Li, Nat. Commun. **11**, 1111 (2020).
[59] Z. Dun, M. Daum, R. Baral, H. E. Fischer, H. Cao, Y. Liu, M. B. Stone, J. A. Rodriguez-Rivera, E. S. Choi, Q. Huang, H. Zhou, M. Mourigal, and B. A. Frandsen, Phys. Rev. B **103**, 064424 (2021).
[60] J. Xiang, C. Su, N. Xi, Z. Fu, Z. Chen, H. Jin, Z. Chen, Z.-J. Mo, Y. Qi, J. Shen, L. Zhang, W. Jin, W. Li, P. Sun, and G. Su, arXiv:2301.03571 [cond-mat.str-el].
[61] A. Jesche, N. Winterhalter-Stocker, F. Hirschberger, A. Bellon, S. Bachus, Y. Tokiwa, A. A. Tsirlin, and P. Gegenwart, Phys. Rev. B **107**, 104402 (2023).
[62] Y. Tokiwa, S. Bachus, K. Kavita, A. Jesche, A. A. Tsirlin, and P. Gegenwart, Commun. Mater. **2**, 42 (2021).
[63] P. Sahebsara and D. Sénéchal, Phys. Rev. Lett. **100**, 136402 (2008).
[64] J. N. Graham, N. Qureshi, C. Ritter, P. Manuel, A. R. Wildes, and L. Clark, Phys. Rev. Lett. **130**, 166703 (2023).
[65] A. Razpopov, D. A. S. Kaib, S. Backes, L. Balents, S. D. Wilson, F. Ferrari, K. Riedl, and R. Valentí, npj Quantum Mater. **8**, 36 (2023).
[66] C. Kim, S. Kim, P. Park, T. Kim, J. Jeong, S. Ohira-Kawamura, N. Murai, K. Nakajima, A. L. Chernyshev, M. Mourigal, S.-J. Kim, and J.-G. Park, Nat. Phys. **19**, 1624 (2023).
[67] C. Wellm, W. Roscher, J. Zeisner, A. Alfonsov, R. Zhong, R. J. Cava, A. Savoyant, R. Hayn, J. van den Brink, B. Büchner, O. Janson, and V. Kataev, Phys. Rev. B **104**, L100420 (2021).
[68] Y.-D. Li, X. Wang, and G. Chen, Phys. Rev. B **94**, 201114(R) (2016).
[69] B. H. Toby, J. Appl. Crystallogr. **34**, 210 (2001).
[70] F. Grußler, M. Hemmida, S. Bachus, Y. Skourski, H.-A. Krug von Nidda, P. Gegenwart, and A. A. Tsirlin, Phys. Rev. B **107**, 224416 (2023).
[71] W. Xie, F. Du, X. Y. Zheng, H. Su, Z. Y. Nie, B. Q. Liu, Y. H. Xia, T. Shang, C. Cao, M. Smidman, T. Takabatake, and H. Q. Yuan, Phys. Rev. B **106**, 075132 (2022).
[72] J. Khatua, Q. P. Ding, M. S. R. Rao, K. Y. Choi, A. Zorko, Y. Furukawa, and P. Khuntia, Phys. Rev. B **108**, 054442 (2023).
[73] X. Kuang, X. Jing, C.-K. Loong, E. E. Lachowski, J. M. S. Skakle, and A. R. West, Chem. Mater. **14**, 4359 (2002).
[74] K. Momma and F. Izumi, J. Appl. Crystallogr. **41**, 653 (2008).
[75] H. D. Zhou, C. Xu, A. M. Hallas, H. J. Silverstein, C. R. Wiebe, I. Umegaki, J. Q. Yan, T. P. Murphy, J.-H. Park, Y. Qiu, J. R. D. Copley, J. S. Gardner, and Y. Takano, Phys. Rev. Lett. **109**, 267206 (2012).
[76] Y. Kamiya, L. Ge, T. Hong, Y. Qiu, D. L. Quintero-Castro, Z. Lu, H. B. Cao, M. Matsuda, E. S. Choi, C. D. Batista, M. Mourigal, H. D. Zhou, and J. Ma, Nat. Commun. **9**, 2666 (2018).
[77] J. A. M. Paddison, M. Daum, Z. Dun, G. Ehlers, Y. Liu, M. B. Stone, H. Zhou, and M. Mourigal, Nat. Phys. **13**, 117 (2017).
[78] U. K. Voma, S. Bhattacharya, E. Kermarrec, J. Alam, Y. M. Jana, B. Sana, P. Khuntia, S. K. Panda, and B. Koteswararao, Phys. Rev. B **104**, 144411 (2021).
[79] Z. W. Cronkwright, M.Sc. thesis, McMaster University, 2020, http://hdl.handle.net/11375/26083.
[80] A. M. Hallas, J. Gaudet, N. P. Butch, M. Tachibana, R. S. Freitas, G. M. Luke, C. R. Wiebe, and B. D. Gaulin, Phys. Rev. B **93**, 100403(R) (2016).
[81] C. Kittel, *Introduction to Solid State Physics* (Wiley, New York, 2005).
[82] E. Gopal, *Specific Heats at Low Temperatures* (Springer, New York, 2012).
[83] G. Sala, M. B. Stone, S.-H. Do, K. M. Taddei, Q. Zhang, G. B. Halász, M. D. Lumsden, A. F. May, and A. D. Christianson, J. Phys.: Condens. Matter **35**, 395804 (2023).

[84] J. Khatua, T. Arh, S. B. Mishra, H. Luetkens, A. Zorko, B. Sana, M. S. R. Rao, B. R. K. Nanda, and P. Khuntia, Sci. Rep. **11**, 6959 (2021).
[85] L. S. Wu, S. E. Nikitin, Z. Wang, W. Zhu, C. D. Batista, A. M. Tsvelik, A. M. Samarakoon, D. A. Tennant, M. Brando, L. Vasylechko, M. Frontzek, A. T. Savici, G. Sala, G. Ehlers, A. D. Christianson, M. D. Lumsden, and A. Podlesnyak, Nat. Commun. **10**, 698 (2019).
[86] Z. M. Song, N. Zhao, H. Ge, T. T. Li, J. Yang, L. Wang, Y. Fu, Y. Z. Zhang, S. M. Wang, J. W. Mei, H. He, S. Guo, L. S. Wu, and J. M. Sheng, Phys. Rev. B **107**, 125126 (2023).
[87] P. Bourgeois-Hope, F. Laliberté, E. Lefrançois, G. Grissonnanche, S. R. de Cotret, R. Gordon, S. Kitou, H. Sawa, H. Cui, R. Kato, L. Taillefer, and N. Doiron-Leyraud, Phys. Rev. X **9**, 041051 (2019).
[88] M.-E. Boulanger, G. Grissonnanche, S. Badoux, A. Allaire, É. Lefrançois, A. Legros, A. Gourgout, M. Dion, C. H. Wang, X. H. Chen, R. Liang, W. N. Hardy, D. A. Bonn, and L. Taillefer, Nat. Commun. **11**, 5325 (2020).
[89] H. Takeda, J. Mai, M. Akazawa, K. Tamura, J. Yan, K. Moovendaran, K. Raju, R. Sankar, K.-Y. Choi, and M. Yamashita, Phys. Rev. Res. **4**, L042035 (2022).
[90] S. Y. Li, J.-B. Bonnemaison, A. Payeur, P. Fournier, C. H. Wang, X. H. Chen, and L. Taillefer, Phys. Rev. B **77**, 134501 (2008).
[91] M. Sutherland, D. G. Hawthorn, R. W. Hill, F. Ronning, S. Wakimoto, H. Zhang, C. Proust, E. Boaknin, C. Lupien, L. Taillefer, R. Liang, D. A. Bonn, W. N. Hardy, R. Gagnon, N. E. Hussey, T. Kimura, M. Nohara, and H. Takagi, Phys. Rev. B **67**, 174520 (2003).
[92] R. C. Zeller and R. O. Pohl, Phys. Rev. B **4**, 2029 (1971).
[93] Z. Zhu, B. Pan, L. Nie, J. Ni, Y. Yang, C. Chen, C. Jiang, Y. Huang, E. Cheng, Y. Yu, J. Miao, A. D. Hillier, X. Chen, T. Wu, Y. Zhou, S. Li, and L. Shu, Innovation **4**, 100459 (2023).
[94] Y. Xu, J. Zhang, Y. S. Li, Y. J. Yu, X. C. Hong, Q. M. Zhang, and S. Y. Li, Phys. Rev. Lett. **117**, 267202 (2016).
[95] S. Lee, W. Lee, K. J. Lee, B. J. Kim, B. J. Suh, H. Zheng, J. F. Mitchell, and K.-Y. Choi, Phys. Rev. B **97**, 104409 (2018).
[96] J. Gaudet, D. D. Maharaj, G. Sala, E. Kermarrec, K. A. Ross, H. A. Dabkowska, A. I. Kolesnikov, G. E. Granroth, and B. D. Gaulin, Phys. Rev. B **92**, 134420 (2015).
[97] P. Dalmas de Réotier, A. Yaouanc, P. C. M. Gubbens, S. Sakarya, E. Jimenez, P. Bonville, and J. A. Hodges, in *HFI/NQI 2004*, edited by K. Maier and R. Vianden (Springer-Verlag, Berlin, 2005), pp. 131–136.
[98] D. Gatteschi and A. Bencini, *EPR of Exchange Coupled Systems* (Springer-Verlag, Berlin, 1990).
[99] A. Abragam and B. Bleaney, *Electron Paramagnetic Resonance of Transition Ions* (Clarendon, Oxford, 1970).
[100] A. Scheie, J. Kindervater, S. Zhang, H. J. Changlani, G. Sala, G. Ehlers, A. Heinemann, G. S. Tucker, S. M. Koohpayeh, and C. Broholm, Proc. Natl. Acad. Sci. USA **117**, 27245 (2020).
[101] S. Onoda and Y. Tanaka, Phys. Rev. B **83**, 094411 (2011).
[102] Y. Shirata, H. Tanaka, A. Matsuo, and K. Kindo, Phys. Rev. Lett. **108**, 057205 (2012).
[103] P. W. Anderson and P. R. Weiss, Rev. Mod. Phys. **25**, 269 (1953).